





## Continuous transition from X- to O-shaped angle-wavelength spectra of a femtosecond filament in a gas mixture

N. A. Panov <sup>1,2,3</sup> D. E. Shipilo <sup>1,2,3</sup> I. A. Nikolaeva,<sup>1,2</sup> V. O. Kompanets <sup>3</sup> S. V. Chekalin,<sup>3</sup> and O. G. Kosareva <sup>1,2,3,\*</sup>

<sup>1</sup>*Faculty of Physics, M. V. Lomonosov Moscow State University, 1/62 Leninskie Gory, Moscow 119991, Russia*

<sup>2</sup>*P. N. Lebedev Physical Institute of the Russian Academy of Sciences, 53 Leninskiy Prospekt, Moscow 119991, Russia*

<sup>3</sup>*Institute of Spectroscopy of the Russian Academy of Sciences, 5 Fizicheskaya, Troitsk, Moscow 108840, Russia*



(Received 7 December 2020; accepted 8 February 2021; published 22 February 2021)

In  $3D + t$  numerical simulations, we propose an experiment wherein a mixture of gases is used for the continuous transition from X- to O-shaped angle-wavelength spectrum of a femtosecond infrared filament. The mixture consists of transparent nitrogen at 40 bar pressure and 85 °C temperature as well as absorbing water vapor at 0–0.36 bar, with the rovibrational resonance at a wavelength slightly longer than the 1.3  $\mu\text{m}$  center of the pump pulse driving the filament. The continuous increase in the water vapor density results in the gas mixture dispersion changing from normal to anomalous and transformation of the short-wavelength conical emission onto on-axis propagating radiation.

DOI: [10.1103/PhysRevA.103.L021501](https://doi.org/10.1103/PhysRevA.103.L021501)

### I. INTRODUCTION

The use of femtosecond laser sources for gas spectroscopy applications, including the diagnostics of the atmosphere [1], combustion [2], and reacting-flow environments [3], requires detailed knowledge of the nonlinear-optical transformation of the pulse in the medium with complex material dispersion. Diagnostics of the atmosphere with a 0.8  $\mu\text{m}$  terawatt Ti:Sapphire laser were performed with white light, which after filamentation propagated in the linear regime up to 4.5 km on the vertical atmospheric path [1]. High-intensity near-infrared radiation at 0.8  $\mu\text{m}$ , for which atmospheric air is highly transparent, experiences nonlinear transformation in the normal dispersion regime. Absorption lines of atmospheric constituents affect the low-intensity part of the supercontinuum and do not alter spatiotemporal distribution of the 0.8  $\mu\text{m}$  pulse in the filament. The angle-wavelength spectrum of near-infrared radiation undergoing filamentation is represented by the colored rings of conical emission in the visible range [4,5] as well as the cone-shaped spectrum in the infrared wing of the supercontinuum [6–8], thus creating an X-shaped angle-wavelength spectrum or X wave [6].

With the development of a 3.9- $\mu\text{m}$ , 80-fs, 20-mJ high-peak-power mid-infrared laser source, the spectral range from 3.2 to 4.2  $\mu\text{m}$  becomes available for the diagnostics of atmospheric constituents [9]. Such powerful pulses propagate through the atmosphere in the nonlinear regime [10] and experience the effect of anomalous group velocity dispersion since the 3.9  $\mu\text{m}$  fundamental laser wavelength is near the asymmetric-stretch rovibrational band of atmospheric carbon dioxide [11].

For the case of ultrashort pulse propagation in a Kerr medium with anomalous group velocity dispersion, the angle-wavelength spectrum of the pulse is predicted to be O shaped [12]. However, registration of such angle-wavelength spectra

with the mid-infrared driver of the filament in air might be challenging. Besides, visualization of the O-shaped spectrum requires reproduction of the spectrum details in the close vicinity of the pump frequency. Recent studies of angle-wavelength spectra in mid-infrared filaments reported on the spatial distributions of the short-wavelength supercontinuum wing and optical harmonics generated by the mid-infrared pump [13,14].

Solids and liquids have broadband regions of normal and anomalous dispersion in their transparency windows [15]. In the experiment [16] an X-shaped angle-wavelength spectrum was obtained in liquid water with 1-ps, 1.6- $\mu\text{J}$ , 0.527- $\mu\text{m}$  pulses in the normal group velocity dispersion regime. By tuning the optical parametric amplifier to 1.055  $\mu\text{m}$  and increasing the initial pulse energy to 14.5  $\mu\text{J}$ , an O-shaped spectrum was obtained in the anomalous dispersion regime. In fused silica the angle-wavelength spectra were observed and simulated in the normal, zero, and anomalous dispersion regimes [10,17].

The study of angle-wavelength spectra of high-peak-power ultrashort pulses at different laser wavelengths raises a question of whether it is possible to design an experiment, in which the angle-wavelength spectrum of the filamenting pulse changes from X to O shaped continuously? While performing this experiment the major parameters of the filament, such as peak intensity, electron density, and length, should remain constant. Indeed, the purpose of this experiment is to explore the effect of dispersion regime variation on the angle-wavelength spectrum, but not the nonlinearity effect.

In this work we propose an experiment wherein a mixture of gases is used for fine control of the continuous transition from an X- to an O-shaped angle-wavelength spectrum in the course of femtosecond mid-infrared pulse filamentation. The major constituent of our gas mixture is nitrogen ( $\text{N}_2$ ), while the minor one is an impurity with rovibrational band in the mid-infrared range. By increasing the density of impurity, while keeping the density of  $\text{N}_2$  constant, we change the

\*kosareva@physics.msu.ru

dispersion from normal to anomalous regime in the short-wavelength vicinity of the absorption band. We aim at the setup [18] primarily. It consists of a high-pressure cuvette allowing the gas temperature rise up to 150 °C corresponding to  $\sim 1$  bar water vapor ( $\text{H}_2\text{O}$ ) pressure, and a tunable laser source with 100-fs pulse, which can be centered at  $\lambda_0 \approx 1.3 \mu\text{m}$ , close to  $\text{H}_2\text{O}$  resonance at  $\sim 1.35 \mu\text{m}$ . We assume that the cuvette is filled with 30 bars of  $\text{N}_2$  and then heated up to  $T = 85^\circ\text{C} = 358 \text{ K}$ . The pressure of  $\text{N}_2$  increases to  $\sim 40$  bar, while its density remains unchanged. The water vapor density is varied in our simulations.

## II. MODEL

Numerical simulations are based on the forward Maxwell equation (FME) [19,20], a paraxial carrier-wave-resolved propagation equation for the time-domain Fourier harmonics  $\hat{E}(\omega, r, z)$  of the electric field  $E(t, r, z)$ :

$$\frac{\partial \hat{E}(\omega)}{\partial z} = -i \left( k(\omega) + \frac{\Delta_{\perp}}{2k(\omega)} \right) \hat{E}(\omega) - \frac{2\pi}{c} \hat{J}(\omega), \quad (1)$$

where  $t$  is the time,  $\omega$  is the angular frequency,  $r$  is the transverse coordinate,  $z$  is the propagation distance,  $c$  is the speed of light in vacuum, and  $\Delta_{\perp} = r^{-1} \partial / \partial r (r \partial / \partial r)$ . Unlike envelope equations, FME adequately describes the resonantly absorbing medium through the full dispersion relation  $k(\omega)$  as well as the absorption due to the delayed nonlinear response [21].

For the pressure and temperature studied, both linear and nonlinear medium responses on the femtosecond timescale depend on the molecular density  $N = pN_0/\theta$  only, where  $N_0 = 2.7 \times 10^{19} \text{ cm}^{-3}$ ,  $\theta = T/273 \text{ K}$ , and pressure  $p$  is in bars. The complex-valued wave number  $k(\omega) = \omega n(\omega)/c$  describes absorption and refraction of the  $\text{N}_2$ - $\text{H}_2\text{O}$  mixture. The refractive index  $n(\omega)$  is given by

$$n(\omega) - 1 = \frac{p_n}{\theta} \times \delta n_n(\omega) + p_w \times \delta n_w(\omega), \quad (2)$$

where  $p_n$  and  $p_w$  are the partial pressures of nitrogen and water vapor, respectively.

The non-resonant term  $\delta n_n(\omega)$  determines the normal dispersion of nitrogen at  $p_n = 1$  bar and temperature 273 K in the mid-infrared range [22]. The term  $\delta n_w(\omega)$  is complex valued; its real and imaginary parts correspond to the resonant dispersion and absorption of  $\text{H}_2\text{O}$ , respectively. The value  $\text{Re}[\delta n_w(\omega)]$  is calculated from  $\text{Im}[\delta n_w(\omega)]$  according to Ref. [23]. We take the data on the absorption index  $\text{Im}[\delta n_w(\omega)]$  of the gas mixture consisting of water vapor and nitrogen at the temperature  $T = 358 \text{ K}$  and  $p_n = 40$  bar from HITRAN database [24]. HITRAN frequency resolution of 300 MHz is distributed onto the numerical grid of our FME solver (resolution of 143 GHz) with preservation of the total absorption inside the band; cf. red and gray curves in Fig. 1(a). Besides, we performed the calculations with the smooth Gaussian shape of the resonance  $\text{Im}[\delta n_w(\omega)]$  and the corresponding refractive index  $\text{Re}[\delta n_w(\omega)]$ ; see Fig. 1(a), blue dashes. Outside the absorption bands at 1.15 and 1.35  $\mu\text{m}$ , the three refraction indices coincide with each other; see Fig. 1(a). Reasonable agreement between the second-order dispersion coefficients  $k_2(\omega) = d^2 \text{Re}[k(\omega)]/d\omega^2$  calculated from the re-

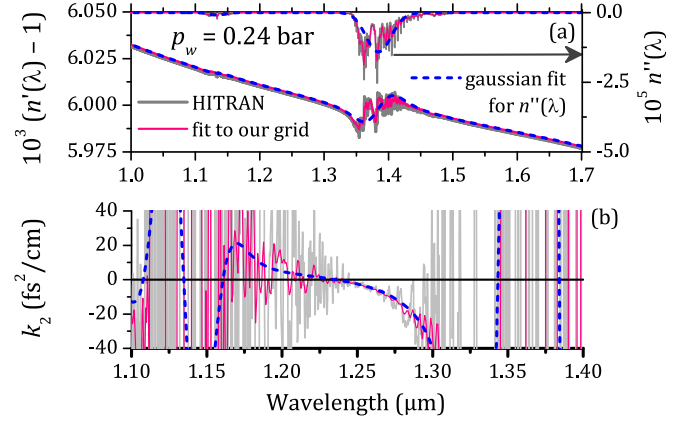


FIG. 1. The dependencies of reflection  $n' = \text{Re}[n]$  [(a), left axis] and absorption  $n'' = \text{Im}[n]$  [(a), right axis] indices as well as second-order dispersion coefficient  $k_2$  (b) on wavelength  $\lambda$ . Gray, red, and blue dashed curves in both panels correspond to the spectroscopic data from HITRAN, the fit of HITRAN data to our grid, and smooth Gaussian absorption respectively.

constructed refractive indices is shown in Fig. 1(b). Note that in the vicinity of our pulse's central wavelength, i.e. in the range 1.20–1.30  $\mu\text{m}$ , the coefficient  $k_2$  calculated from Gaussian fit of the absorption line shows the change of the dispersion from normal to anomalous regime explicitly and allows us to define the zero group velocity dispersion point as  $\lambda^{(k_2=0)} \approx 1.23 \mu\text{m}$  for  $p_w = 0.24$  bar [Fig. 1(b), blue dashed curve].

The nonlinear current  $J(t) = J_{\text{free}} + J_{\text{abs}} + \partial_t P^{(3)}$  accommodates the free electron current  $J_{\text{free}}(t)$  defined as

$$\partial_t J_{\text{free}}(t) = (e^2/m_e) N_e(t) E(t) - \nu_c J_{\text{free}}(t), \quad (3)$$

where  $e$  and  $m_e$  are electron charge and mass, and  $\nu_c \approx (p_n/\theta) \times 5 \text{ ps}^{-1}$  is the electron-neutral collision rate; the absorption current  $J_{\text{abs}}(t) = -W_I \partial_t N_e(t)/E(t)$ , where  $W_I$  is the ionization potential of a component and  $N_e(t)$  is free electron density. The third-order polarization includes both instantaneous and delayed rotational responses:

$$P^{(3)}(t) = \chi^{(3)} E(t) \left( E^2(t) + \int_{-\infty}^t K(t-t') E^2(t') dt' \right), \quad (4)$$

where  $\chi^{(3)}$  corresponds to Kerr coefficient  $n_2 = (p_n/\theta) \times 10^{-19} \text{ cm}^2/\text{W}$ , and  $K(t)$  is the normalized kernel calculated according to [25].

We neglect the possible resonant nonlinear response of water vapor. To date, experiments with laser drivers close to the absorption bands of water [18] or carbon dioxide [9] have not indicated any noticeable effect of the resonant nonlinear response on the mid-infrared filamentation scenario. Recently, a harshly truncated representation of the water rovibrational nonlinearity was implemented in propagation simulations [26]. According to this study, the 7- $\mu\text{m}$   $\text{H}_2\text{O}$  band provides a 20% addition to the air nonlinearity for a 10- $\mu\text{m}$  100-fs pulse with intensity below 10  $\text{TW}/\text{cm}^2$  if the water vapor density constitutes 1% of the air density. In our simulations, we remain below 1% density of the impurity and consider the transitions at 1.35  $\mu\text{m}$  with the oscillator strength  $\sim 100$  times lower than the one at 7  $\mu\text{m}$  wavelength [24].

We used the rate equation for the plasma density  $N_e$ ,

$$\partial_t N_e(t) = w(E)[N - N_e(t)], \quad (5)$$

with tunneling ionization rate  $w(E)$  and molecule number density  $N$ . Equation (5) does not include the contribution from the avalanche ionization (term  $\propto N_e$ ). In our conditions of the infrared pulse filamentation the kinetic energy of a free electron,  $W_k \propto E^2(t)\lambda^2$ , reaches several tens of electronvolts twice within the optical period, i.e.,  $W_k > W_I$ . The commonly used theory of avalanche ionization assumes  $W_k < W_I$  and multiple elastic electron-neutral collisions prior to the ionizing one [27]. We estimate the avalanche addition to ionization based on the analysis of mean kinetic energy of an electron in the laser field extracted from simulations, and we propose that in our conditions the avalanche mechanism is suppressed due to the short-wavelength shift of the trailing edge of the pulse, thus decreasing the kinetic energy dramatically [28].

### III. TUNING PULSE WAVELENGTH TO ANOMALOUS DISPERSION REGION

The laser system used in our experiments [18] is tunable, so we can choose the pulse central wavelength  $\lambda_0 < 1.35 \mu\text{m}$ . The steel cuvette [18] is safe up to a pressure of 100 bar. So, for the given  $\lambda_0$ , we can choose the optimal nitrogen pressure  $p_n$  and water vapor pressure  $p_w$ . The dependence of the critical power for self-focusing  $P_{\text{cr}}$  for  $\lambda_0 = 1.2\text{--}1.35 \mu\text{m}$  on the pressure  $p_n$  is [29]

$$P_{\text{cr}} \approx (\theta/p_n) \times 25 \text{ GW}. \quad (6)$$

The peak power of the laser facility [18] in this range of  $\lambda_0$  is  $P \approx 2.5 \text{ GW}$  (corresponding to  $150 \mu\text{J}$  energy and 60 fs duration). So, the pressure  $p_n > 13 \text{ bar}$  is required to produce a single filament.

Despite the complicated structure of  $\text{H}_2\text{O}$  resonances, the transition from normal to anomalous dispersion ( $k_2 = 0$ ) at  $\lambda^{(k_2=0)} \approx 1.23 \mu\text{m}$  (for  $p_w = 0.24 \text{ bar}$ ) is clearly seen in Fig. 1(b). We calculated the wavelength  $\lambda^{(k_2=0)}$  for different water vapor pressures  $p_w$  [Fig. 2(a), black curve]. In the experiment [18] the pulse spectrum was Gaussian with a width of  $\sim 100 \text{ nm}$ . We chose the central wavelength of  $1.3 \mu\text{m}$ , so the major part of the spectrum [filled area in Fig. 2(a)] is within the anomalous dispersion region [area between black solid curve and orange dashed line in Fig. 2(a)] for pressures  $p_w \geq 0.24 \text{ bar}$ .

In simulations a pulse with central wavelength  $\lambda_0 = 1.3 \mu\text{m}$  undergoes filamentation in a gas mixture of  $p_n = 40 \text{ bar}$  molecular nitrogen at a temperature  $T = 358 \text{ K}$  and water vapor with a pressure varying from 0 to 0.36 bar. Other pulse parameters are taken from the experiment [18]: pulse duration and energy were 60 fs and  $120 \mu\text{J}$ , respectively. Beam diameter and geometrical focusing distance of the lens were 2 mm and 30 cm, respectively.

### IV. TRANSITION FROM X- TO O-SHAPED SPECTRA WITH HUMIDITY VARIATION

We will follow the change of the angle-wavelength spectrum in a mixture of  $\text{N}_2$  with a fixed pressure  $p_n = 40 \text{ bar}$  and  $\text{H}_2\text{O}$  with a pressure  $p_w$  varied from 0 to 0.36 bar

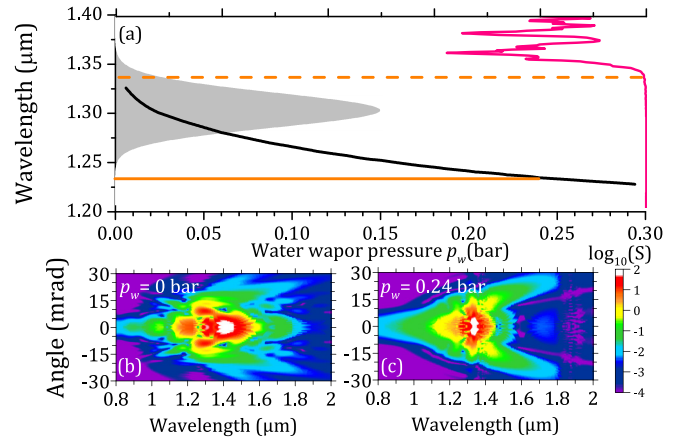


FIG. 2. (a) Dependence of the wavelength  $\lambda^{(k_2=0)}$  corresponding to zero dispersion on water vapor pressure (black curve). The gray filled Gaussian profile indicates the initial pulse spectrum. The absorption coefficient is shown by the red curve. The orange dashed line is a border of absorption band, the orange solid line indicates the wavelength of zero dispersion at  $p_w = 0.24 \text{ bar}$ . Angle-wavelength distributions for (b) dry ( $p_w = 0 \text{ bar}$ , normal dispersion) and (c) humid ( $p_w = 0.24 \text{ bar}$ , anomalous dispersion) nitrogen.

[cf. Figs. 2(b) and 2(c)]. To attribute the changes in the angle-wavelength spectrum from X to O shaped to the transition from normal to anomalous dispersion strictly, we need the high-intensity filament and the corresponding plasma channel to depend on the humidity in the cuvette weakly.

Indeed, as the pressure  $p_w$  increases from 0 to 0.24 bar, the filament peak intensity drops down by 8% only [Fig. 3(a), stars, decrease from 284 to 261  $\text{TW}/\text{cm}^2$ ]. The peak electron density follows the intensity and drops by 33% [Fig. 3(a), open circles, from  $4.32 \times 10^{18}$  to  $2.93 \times 10^{18} \text{ cm}^{-3}$ ]. This 33% drop is negligible in comparison with, for example, two orders of magnitude decrease in the plasma density measurements performed with the numerical aperture decrease by a factor

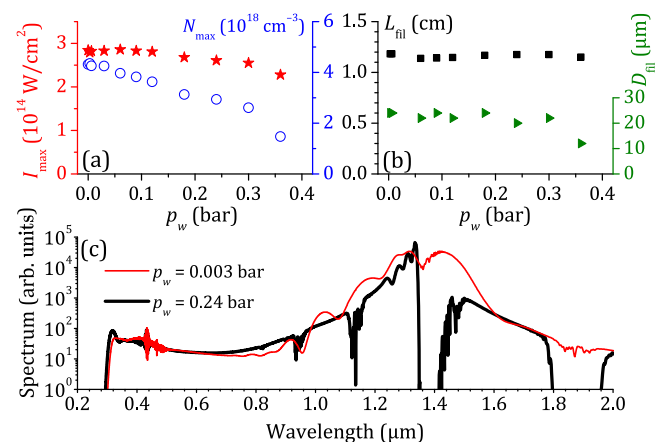


FIG. 3. Dependence on the water vapor pressure of (a) maximal intensity  $I_{\text{max}}$  (red stars, left axis) and maximal plasma density  $N_{\text{max}}$  (blue open circles, right axis) in the filament, and (b) length  $L_{\text{fil}}$  (black squares, left axis) and diameter  $D_{\text{fil}}$  (green triangles, right axis) of the plasma channel. (c) Supercontinuum spectra for two water vapor pressures at the end of the cuvette,  $z = 60 \text{ cm}$ .

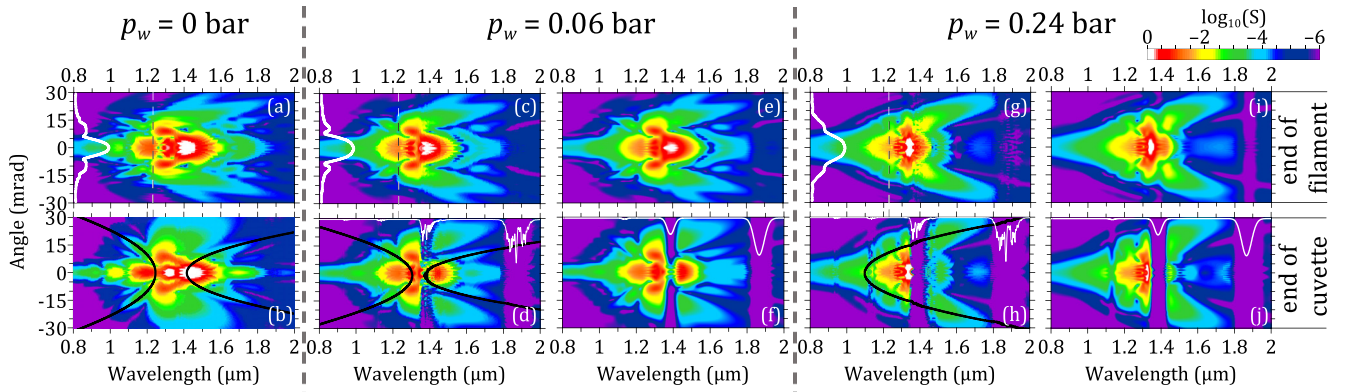


FIG. 4. Angle-wavelength spectra demonstrating transition from X to O waves under water vapor pressure increase from (a),(b)  $p_w = 0$  bar (dry nitrogen, normal dispersion) through (c)–(f)  $p_w = 0.06$  bar (humid nitrogen, weak anomalous dispersion) to (g)–(j)  $p_w = 0.24$  bar (humid nitrogen, anomalous dispersion). White curves in (a), (c), (g) show the angular distributions at  $1.23 \mu\text{m}$  (vertical dashed lines). Spectra in the upper row are just after the end of the filament; spectra in the lower row are at the end of the cuvette. Black curves fit the angle-wavelength spectra with the quasi-phase-matching relations [31]. Panels (c), (d), (g), (h) show the results of simulations with the absorption coefficient (white curves) from the HITRAN database fitted on our grid, and panels (e), (f), (i), (j) show the results with smooth Gaussian shape of the resonance.

of 4 [30]. The plasma channel length and diameter estimated at the level of  $8 \times 10^{14} \text{ cm}^{-3}$  are fairly constant and equal to 1.2 cm and  $\sim 23 \mu\text{m}$ , respectively [Fig. 3(b)]. The supercontinuum width and intensity are identical in this range of water vapor pressure [Fig. 3(c)]. Overall, the filament characteristics are almost insensitive to the humidity up to  $p_w = 0.24$  bar introduced into the high-pressure nitrogen. For  $\text{H}_2\text{O}$  pressure  $p_w > 0.24$  bar the variation of filament parameters tends to increase [Fig. 3(a)].

Transition from X- to O-shaped spectra of a mid-infrared pulse in the mixture of molecular nitrogen and water vapor occurs continuously with gradual water vapor pressure increase (Fig. 4, upper row). The X-shaped angle-wavelength spectrum in dry nitrogen exhibits rings on the short-wavelength side,  $1 < \lambda < \lambda_0 = 1.3 \mu\text{m}$  [Fig. 4(a)]. Degradation of these rings might be revealed explicitly by comparing the cross sections of the angle-wavelength distributions at  $\lambda = 1.23 \mu\text{m}$ , corresponding to the zero dispersion at  $p_w = 0.24$  bar [Figs. 4(a), 4(c), 4(g) white solid curves]. Note specifically the decrease in spectral intensity of the local maximum at the angle of  $\sim 10$  mrad in Fig. 4(a) as compared with Figs. 4(c) and 4(g). Thus, as the water vapor pressure reaches  $p_w = 0.24$  bar, predominantly on-axis propagation of the near-infrared spectral components, or transition to the O-shaped spectrum, is attained [Fig. 4(g)]. Meanwhile, the rings on the longer-wavelength side of the spectrum became more and more pronounced with increasing humidity since for  $\lambda > 1.5 \mu\text{m}$  the normal dispersion regime dominates the propagation [cf. Figs. 4(a) and 4(g)].

Potential registration of the X- to O-shaped transition of the angle-wavelength spectrum requires simulation data on the spectral intensity distribution not only right after the  $\sim 1.2$ -cm filament (Fig. 4, upper row,  $z = 31$  cm), but also at the exit of the gas cuvette (Fig. 4, lower row,  $z = 60$  cm). After the end of the plasma channel, the quasilinear propagation of the pulse preserves the angle-wavelength spectrum except for the depletion of intensity at absorption bands [cf. Figs. 4(c), 4(g)

with Figs. 4(d), 4(h) respectively]. Note that the small-scale details of the complex water molecule resonance structure have minor influence on the angle-wavelength spectrum outside the band [cf. the panels of the lower row in Fig. 4: (d) with (f) and (h) with (j)]. Thus, continuous change of the dispersion regime from normal to the anomalous one might be detected through the registration of the angle-wavelength spectrum after  $\sim 30$  cm of propagation in high-pressure humid nitrogen.

## V. CONCLUSIONS

In conclusion, we proposed to use the gas mixture with variable group velocity dispersion consisting of  $\text{N}_2$  (40 bar) and  $\text{H}_2\text{O}$  (0–0.36 bar, absorption resonance at  $1.35 \mu\text{m}$ ) at the temperature of  $85^\circ\text{C}$  in order to control the nonlinear-optical transformation of a  $1.3\text{-}\mu\text{m}$  60-fs pulse undergoing filamentation. The filament parameters (intensity, plasma density, plasma channel length, and diameter) change weakly with the variation of the water vapor density. In contrast, the spatially resolved supercontinuum spectrum of the pulse strongly depends on the density of water vapor: the continuous transition from normal dispersion of dry nitrogen to anomalous dispersion of the humid case corresponds to the continuous transition from X- to O-shaped angle-wavelength spectrum. After the end of the plasma channel, the quasilinear propagation of the pulse preserves the angle-wavelength spectrum except for the depletion of intensity at absorption bands. Thus, the registration of such angle-wavelength spectra is possible in the experiment. Similar experiment can be performed by using carbon dioxide instead of water vapor and a longer wavelength pump in the mid-infrared.

## ACKNOWLEDGMENT

We are thankful for financial support from the Russian Science Foundation (Grant No. 18-12-00422).

- [1] J. Kasparian, M. Rodríguez, G. Méjean, J. Yu, E. Salmon, H. Wille, R. Bourayou, S. Frey, Y.-B. André, A. Mysyrowicz *et al.*, White-light filaments for atmospheric analysis, *Science* **301**, 61 (2003).
- [2] H.-L. Li, H.-L. Xu, B.-S. Yang, Q.-D. Chen, T. Zhang, and H.-B. Sun, Sensing combustion intermediates by femtosecond filament excitation, *Opt. Lett.* **38**, 1250 (2013).
- [3] A. K. Patnaik, H. U. Stauffer, P. S. Hsu, N. Jiang, P. J. Wrzesinski, and S. Roy, Ultrafast diagnostics of reacting flows and plasmas, in *8TH BSME International Conference on Thermal Engineering, 19–21 December 2018, Dhaka, Bangladesh*, edited by A. K. M. Sadrul Islam, M. Ruhul Amin, and M. Ali, AIP Conf. Proc. No. 2121 (AIP, New York, 2019), p. 020003.
- [4] E. Nibbering, P. Curley, G. Grillon, B. Prade, M. Franco, F. Salin, and A. Mysyrowicz, Conical emission from self-guided femtosecond pulses in air, *Opt. Lett.* **21**, 62 (1996).
- [5] O. Kosareva, V. Kandidov, A. Brodeur, C. Chien, and S. Chin, Conical emission from laser–plasma interactions in the filamentation of powerful ultrashort laser pulses in air, *Opt. Lett.* **22**, 1332 (1997).
- [6] D. Faccio, A. Averchi, A. Lotti, P. Di Trapani, A. Couairon, D. Papazoglou, and S. Tzortzakis, Ultrashort laser pulse filamentation from spontaneous X wave formation in air, *Opt. Express* **16**, 1565 (2008).
- [7] F. Théberge, M. Châteauneuf, V. Ross, P. Mathieu, and J. Dubois, Ultrabroadband conical emission generated from the ultraviolet up to the far-infrared during the optical filamentation in air, *Opt. Lett.* **33**, 2515 (2008).
- [8] D. Shipilo, D. Pushkarev, N. Panov, D. Uryupina, V. Andreeva, R. Volkov, A. Balakin, A. Shkurinov, I. Babushkin, U. Morgner *et al.*, Near-infrared conical emission from 800 nm filament in air, *Laser Phys. Lett.* **14**, 035401 (2017).
- [9] A. V. Mitrofanov, A. A. Voronin, D. A. Sidorov-Biryukov, A. Pugžlys, E. A. Stepanov, G. Andriukaitis, S. Ališauskas, T. Flóry, A. B. Fedotov, A. Baltuška, and A. M. Zheltikov, Mid-infrared laser filaments in the atmosphere, *Sci. Rep.* **5**, 8368 (2015).
- [10] S. V. Chekalin, A. E. Dokukina, A. E. Dormidonov, V. O. Kompanets, E. O. Smetanina, and V. P. Kandidov, Light bullets from a femtosecond filament, *J. Phys. B* **48**, 094008 (2015).
- [11] A. Mitrofanov, A. Voronin, D. Sidorov-Biryukov, M. Rozhko, E. Stepanov, A. Fedotov, V. Shumakova, S. Ališauskas, A. Pugžlys, A. Baltuška *et al.*, Mapping anomalous dispersion of air with ultrashort mid-infrared pulses, *Sci. Rep.* **7**, 2103 (2017).
- [12] L. W. Liou, X. D. Cao, C. J. McKinstrie, and G. P. Agrawal, Spatiotemporal instabilities in dispersive nonlinear media, *Phys. Rev. A* **46**, 4202 (1992).
- [13] A. V. Mitrofanov, A. A. Voronin, D. A. Sidorov-Biryukov, S. I. Mitryukovsky, M. V. Rozhko, A. Pugžlys, A. B. Fedotov, V. Y. Panchenko, A. Baltuška, and A. M. Zheltikov, Angle-resolved multioctave supercontinua from mid-infrared laser filaments, *Opt. Lett.* **41**, 3479 (2016).
- [14] X. Ren, Y. Wang, Z. Chang, J. Welch, A. Bernstein, M. Downer, J. Brown, M. Gaarde, A. Couairon, M. Kolesik *et al.*, In-Line Spectral Interferometry in Shortwave-Infrared Laser Filaments in Air, *Phys. Rev. Lett.* **123**, 223203 (2019).
- [15] A. Dubietis, G. Tamošauskas, R. Šuminas, V. Jukna, and A. Couairon, Ultrafast supercontinuum generation in bulk condensed media, *Lith. J. Phys.* **57**, 113 (2017).
- [16] M. A. Porras, A. Dubietis, E. Kučinskas, F. Bragheri, V. Degiorgio, A. Couairon, D. Faccio, and P. Di Trapani, From X-to O-shaped spatiotemporal spectra of light filaments in water, *Opt. Lett.* **30**, 3398 (2005).
- [17] V. Kandidov, E. Smetanina, A. Dormidonov, V. Kompanets, and S. Chekalin, Formation of conical emission of supercontinuum during filamentation of femtosecond laser radiation in fused silica, *J. Exp. Theor. Phys.* **113**, 422 (2011).
- [18] V. Kompanets, D. Shipilo, I. Nikolaeva, N. Panov, O. Kosareva, and S. Chekalin, Nonlinear enhancement of resonance absorption at the filamentation of a mid-infrared pulse in high-pressure gases, *JETP Lett.* **111**, 31 (2020).
- [19] A. V. Husakou and J. Herrmann, Supercontinuum Generation of Higher-Order Solitons by Fission in Photonic Crystal Fibers, *Phys. Rev. Lett.* **87**, 203901 (2001).
- [20] M. Kolesik and J. V. Moloney, Nonlinear optical pulse propagation simulation: From Maxwell’s to unidirectional equations, *Phys. Rev. E* **70**, 036604 (2004).
- [21] N. A. Panov, D. E. Shipilo, A. M. Saletsky, W. Liu, P. G. Polynkin, and O. G. Kosareva, Nonlinear transparency window for ultraintense femtosecond laser pulses in the atmosphere, *Phys. Rev. A* **100**, 023832 (2019).
- [22] E. R. Peck and B. N. Khanna, Dispersion of nitrogen, *J. Opt. Soc. Am.* **56**, 1059 (1966).
- [23] N. A. Panov, D. E. Shipilo, V. A. Andreeva, O. G. Kosareva, A. M. Saletsky, H. Xu, and P. Polynkin, Supercontinuum of a 3.9- $\mu\text{m}$  filament in air: Formation of a two-octave plateau and nonlinearly enhanced linear absorption, *Phys. Rev. A* **94**, 041801(R) (2016).
- [24] L. Rothman, I. Gordon, Y. Babikov *et al.*, The HITRAN2012 molecular spectroscopic database, *J. Quant. Spectrosc. Radiat. Transfer* **130**, 4 (2013).
- [25] P. A. Oleinikov and V. T. Platonenko, Raman transitions between rotational levels and self-phase modulation of subpicosecond light pulses in air, *Laser Phys.* **3**, 618 (1993).
- [26] P. Rosenow, P. Panagiotopoulos, M. Kolesik, S. W. Koch, and J. V. Moloney, Nonlinear rovibrational response in the propagation of long-wavelength infrared pulses and pulse trains, *J. Opt. Soc. Am. B* **36**, 3457 (2019).
- [27] Y. P. Raizer and J. E. Allen, *Gas Discharge Physics* (Springer, Berlin, 1997).
- [28] See Supplemental Material at <http://link.aps.org/supplemental/10.1103/PhysRevA.103.L021501> for the estimations of avalanche ionization efficiency in our conditions. The following references are cited in the Supplemental Material [32–35].
- [29] J. M. Brown, A. Couairon, and M. B. Gaarde, *Ab initio* calculations of the linear and nonlinear susceptibilities of N<sub>2</sub>, O<sub>2</sub>, and air in midinfrared laser pulses, *Phys. Rev. A* **97**, 063421 (2018).
- [30] F. Théberge, W. Liu, P. T. Simard, A. Becker, and S. L. Chin, Plasma density inside a femtosecond laser filament in air: Strong dependence on external focusing, *Phys. Rev. E* **74**, 036406 (2006).
- [31] M. Kolesik and J. V. Moloney, Perturbative and non-perturbative aspects of optical filamentation in bulk dielectric media, *Opt. Express* **16**, 2971 (2008).

- [32] A. Couairon and A. Mysyrowicz, Femtosecond filamentation in transparent media, *Phys. Rep.* **441**, 47 (2007).
- [33] E. M. Wright, S. W. Koch, M. Kolesik, and J. V. Moloney, Memory effects in the long-wave infrared avalanche ionization of gases: A review of recent progress, *Rep. Prog. Phys.* **82**, 064401 (2019).
- [34] K. Schuh, M. Kolesik, E. M. Wright, J. V. Moloney, and S. W. Koch, Self-Channeling of High-Power Long-Wave Infrared Pulses in Atomic Gases, *Phys. Rev. Lett.* **118**, 063901 (2017).
- [35] D. A. Romanov, X. Gao, A. L. Gaeta, and R. J. Levis, Intrapulse impact processes in dense-gas femtosecond laser filamentation, *Phys. Rev. A* **97**, 063411 (2018).